SUPPLEMENTARY INFORMATION FOR

Overlooking probabilistic mapping renders urban flood risk management inequitable

José M. Bodoque[1*]; Álvaro Esteban-Muñoz[1*]; Juan A. Ballesteros-Cánovas[2]

[1]Department of Mining and Geological Engineering, University of Castilla-La Mancha, UCLM, Av. Carlos III s/n, 45071, Toledo, Spain

[2]National Museum of Natural Sciences, Spanish Research Council, MNCN-CSIC, C/ Serrano 115bis, 28006, Madrid, Spain

***Corresponding authors:** José M. Bodoque (JoseMaria.Bodoque@uclm.es)

Álvaro Esteban-Muñoz (em.alvaro.l@gmail.com)

Supplementary Information

Supplementary Notes 1 to 7

Supplementary Figs. 1 to 5

Supplementary Note 1: Flood quantile estimation procedure.

First, we visually checked the peak-flow time series plot to identify any potential data errors. Following that, 47 maximum instantaneous flow data (MIF) were identified. In addition, the available time series comprised 32 maximum mean flow values that were converted to MIF via linear regression between pairs of data. Consequently, a continuous 76-year MIF time series encompassing the years 1942 to 2018 was obtained, along with three isolated years of MIF for the years 1912 to 1952. When performing flood frequency analysis, we statistically examined the data for conformity with the underlying assumptions (i.e., stationarity, homogeneity, and independence). We used two statistical tests for stationarity (Dickey-Fuller and Augmented Dickey Fuller), one for homogeneity (Pettitt), and two statistical tools for independence (autocorrelation and partial autocorrelation functions).

Second, we applied Bulletin 17C guidelines, which describe flood frequency analysis data and procedures[1]. The flood frequency analysis conducted in this analysis was based on the Pearson type III distribution with logarithmic transformation of flow data (Supplementary Note 1)[1]. Using the Expected Moments Algorithm (EMA) relying on the generalized method of moments procedure[2] and the station skew coefficient automatically estimated by the process, the parameters of this distribution were estimated, allowing the emphasis to be on the at-site data. Multiple Grubbs-Beck test were applied to separate potentially influential low flows from flood frequency analysis[2]. The flood quantile confidence intervals were calculated using EMA and all available data, including potentially influential low flows and at-site skew. The analysis considered the 90% confidence interval (5-percent CL and 95-percent CL).

Thirdly, we consider three flood quantiles (0.05 CL, fitted value, and 0.95 CL) corresponding to the 500-year flood. Such quantiles were propagated 40 km downstream from the flow gauge with a statistically significant MIF time series to the upstream boundary condition of the hydraulic model implemented at the study site. To do this, we coupled the MOHID model[3] to simulate alluvial aquifer-river interaction and the HEC-RAS model, aiming to assess water storage on the floodplain[4]. To achieve a trustworthy geometry for the 2D mesh, for HEC-RAS, and the 3D mesh, for MOHID, we used open-source information to define underground data (i.e., alluvial aquifer geology and soil characteristics) and terrain (i.e., LiDAR data), and surface structures (i.e., rural roads and irrigation channels layer vector). Finally, propagated values were used to create a triangular distribution, where the minimum and maximum known values were matched to 0.05 CL and 0.95 CL, respectively. The estimated central value of the triangular distribution was analogous to the value of the flood quantile defined by the log Pearson Type III distribution computed curve.

Supplementary Note 2: **Log-Pearson Type III Probability Distribute Function**

$$f\ (\tau, \alpha, \beta) = \frac{\left(\frac{x-\tau}{\beta}\right)^{\alpha-1} exp\left(-\frac{x-\tau}{\beta}\right)}{|\beta|\Gamma(\alpha)}$$

Where τ is the location parameter; α is the shape parameter and is positive; β is the scale parameter; $\Gamma(\alpha)$ is the gamma function $\int_0^{\infty} \quad t\hat{}(\alpha-1)\ exp(-t)dt$; and $\left(\frac{x-\tau}{\beta}\right)^{\alpha-1}$ is ≥ 0.

Supplementary Note 3: Additional notes about Stochastics flood maps

The output map sets of flood depths and flow velocities were processed to create five different types of stochastic maps for the 500-year flood. We used a common cell-by-cell process in all cases, which included (i) collecting all possible depth and/or velocity values for a unique cell; (ii) a specific calculation process that was different for each desired result; and (iii) repeating the process until we processed all cells, thus covering the entire map. Instead of conducting this operation in a linear, cell-by-cell manner, we perform it simultaneously using multiprocessing techniques. We created the following maps using this method: (1) convergence maps; (2) sensitivity maps; (3) a probability flood inundation map; (4) depth and velocity stochastic maps; and (5) a flood hazard stochastic map.

Initially, the convergence and sensitivity maps were generated according to the procedure outlined in the materials and methods section. Second, the probability map depicts the probability of a cell being flooded, regardless of the water depth reached. In all simulations, the specific calculation process for this map consisted of determining whether a given cell was flooded. The probability of flooding was then determined by dividing the number of times it was flooded by the total number of simulations.

The depth and velocity stochastic maps employed more expensive computational techniques. To generate these maps, a non-parametric kernel density estimation[5] was applied to an empirical probability distribution function (Supplementary Note 7). Due to the availability of sufficient data, it was not necessary to calibrate the kernel density estimation parameters, which allowed us to adjust them. Using the Scott's Rule[6], the bandwidth selection was automatically estimated, enabling the Gaussian kernel for each cell to be automatically estimated.

Supplementary Note 4. Additional notes about the latin hypercube sampling method

After selecting the most appropriate probability distribution function for each input data, we followed a common process to adjust latin hypercube sampling to each input data: (1) generate a latin hypercube sampling between 0 and 1 (e.g., 500 values between 0 and 1); (2) transform the probability distribution function into the appropriate cumulative distribution function; (3) assess the 0-1 sample in the cumulative distribution function, providing the values for the MC procedure (e.g., 500 values between the peak flows range for the 500-year flood).

Supplementary Note 5: High resolution DBM.

To build the DBM, 32 cross-sections were taken over a 5-kilometer reach of the urban Duero River in Zamora. To this end, we employed a single-beam echosounder embedded in an aquatic drone (sub-centimetric accuracy), taking into account man-made structures (such as bridges and weirs) and the geomorphological configuration of the reach, particularly in areas where islands and bars are present. We interpolated and modified the domain between these cross-sections based on the identification of critical erodible zones (e.g., owing to bridge scour) and possible sediment aggregation zones (e.g., upstream of weirs). Then, a survey for bathymetric error assessment was conducted using the same single-beam echosounder device that was used to get the cross-sections, which collected independent control points between them. Thus, we gathered over 10,000 bathymetric independent control points along the studied river reach. To assess the inaccuracy in the DBM, we conducted a two-step geostatistical analysis. To do this, after computing the differences between the DBM and the independent control points, we applied a Johnson transformation to all points to validate that they followed a normal distribution. Then, we investigated trends, autocorrelation, and semi-variogram plots in accordance with the geostatistical analysis's best fit. The procedure was concluded when the mean standard error was close to zero, the root-mean-square standard error was close to one, and the average standard error and root-mean-square error were as small as possible.

Supplementary Note 6: High resolution DSM

We utilized LiDAR data (downloaded from the National Center for Geographic Information of the Spanish National Geographic Institute) with a vertical root mean square error of 0.2 meters and an average point density of 0.5 points per square meter. This data was filtered by separating ground points and points representing human-made features (e.g., buildings, walls, and streets) from the point cloud. Subsequently, the DSM was created, which included buildings, walls, and streets (Supplementary Fig. 5). In order to quantify the DSM's inaccuracy, we then conducted a

DGPS survey that delivered 3,412 independent control points. These independent control points were largely placed in urban areas, but also in periurban zones and the entire floodplain. To quantify the DSM error, we used the same geostatistical method as outlined in Supplementary Note 5.

Supplementary Note 7: Kernel density estimation formula

$$f\ (\tau,\alpha,\beta) = \frac{\left(\frac{x-\tau}{\beta}\right)^{\alpha-1} exp\left(-\frac{x-\tau}{\beta}\right)}{|\beta|\Gamma(\alpha)}$$

Where τ is the location parameter; α is the shape parameter and is positive; β is the scale parameter; $\Gamma(\alpha)$ is the gamma function $\int_0^\infty t\hat{}(\alpha-1)\ exp(-t)dt$; and $\left(\frac{x-\tau}{\beta}\right)^{\alpha-1}$ is ≥ 0.

Supplementary Fig.1. HEC-RAS Model characteristics and location. It depicts the DSM from which the 2D calculation mesh was derived, the location of the boundary conditions for the hydraulic model, and the extent of the land use map used to characterize roughness. The orthoimages were obtained from the Spanish National Center for Geographic Information.

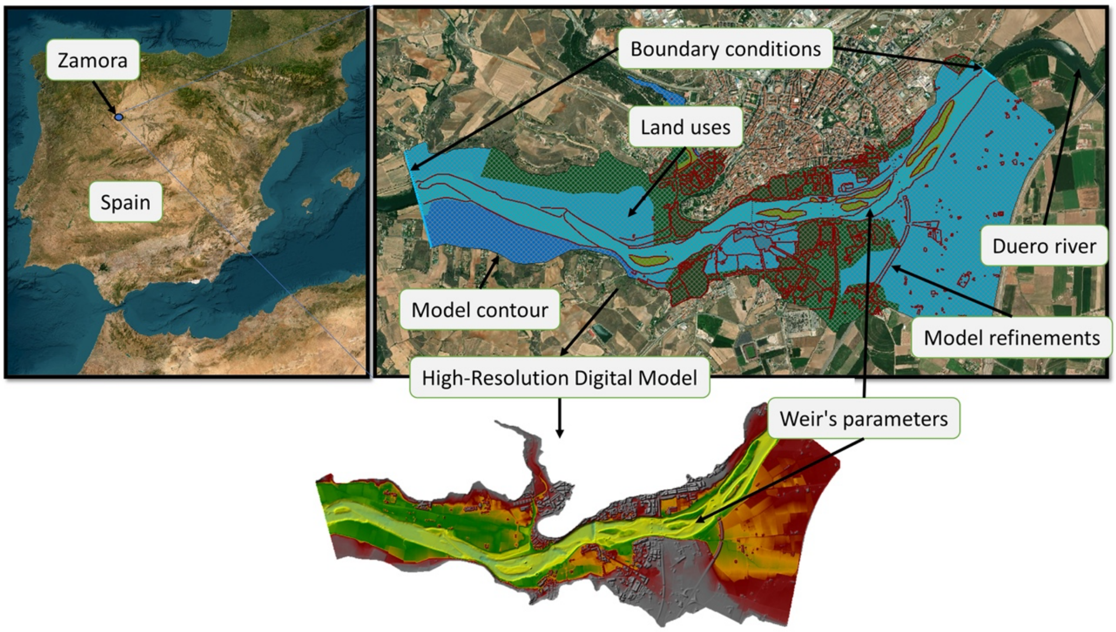

Supplementary Fig.2. Water depth and flow velocity output sensitivity maps resulting from a global sensitivity analysis of the stochastic flood hazard model (500-year flood) for each ranking position. The black contour delimits the stochastic water depth and flow velocity outputs. The included legend shows how the SI fluctuates over the whole examined domain for each input factor, with lighter hues of the same color corresponding to lower SI values and darker shades corresponding to higher SI values. The orthoimages were obtained from the Spanish National Center for Geographic Information.

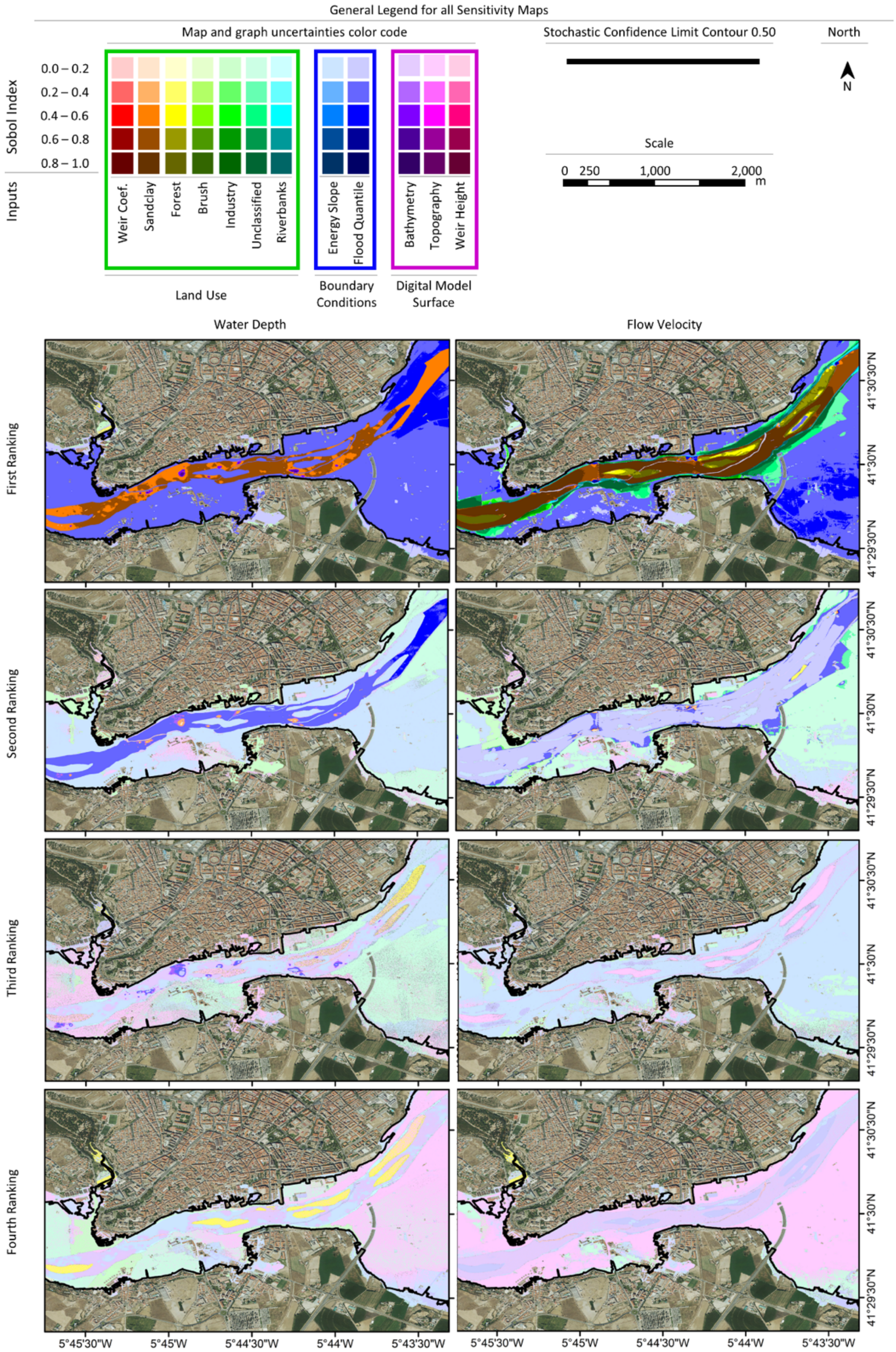

Supplementary Fig. 3. Stochastic flow velocity map corresponding to the 500-year flood. The limits or contours of the deterministic flood area and stochastically produced flooding are displayed, taking into consideration both the 0.95 CL and the 0.05 CL. The orthoimage was obtained from the Spanish National Center for Geographic Information.

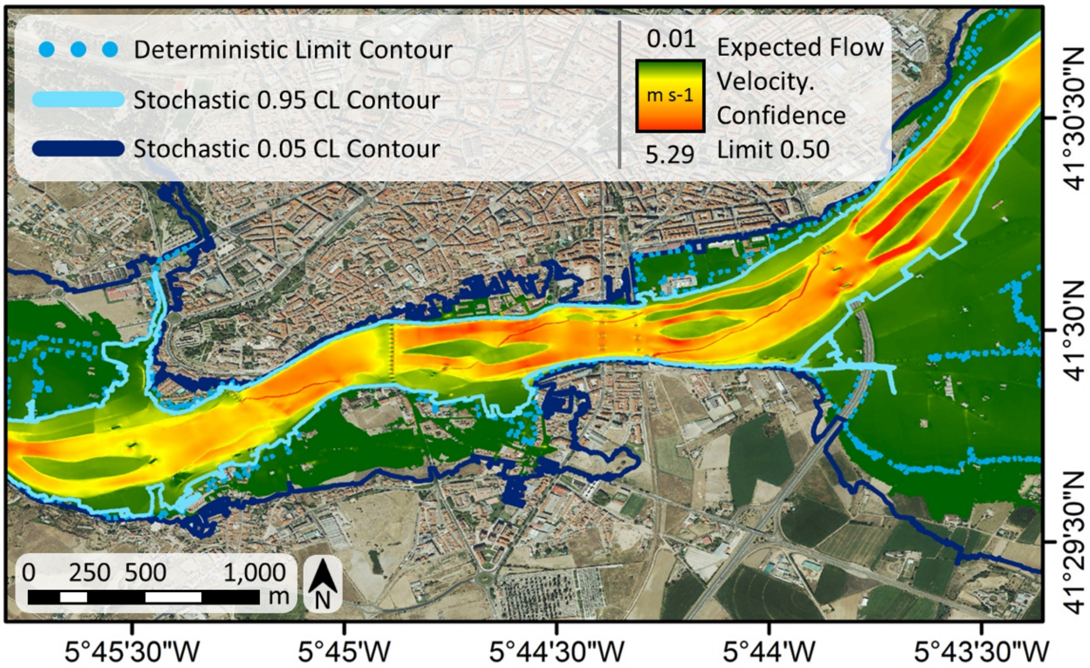

Supplementary Fig. 4. Flow Gauge Data and Log Pearson Type-III fit. Flood frequency analysis was conducted considering systematic data alone.

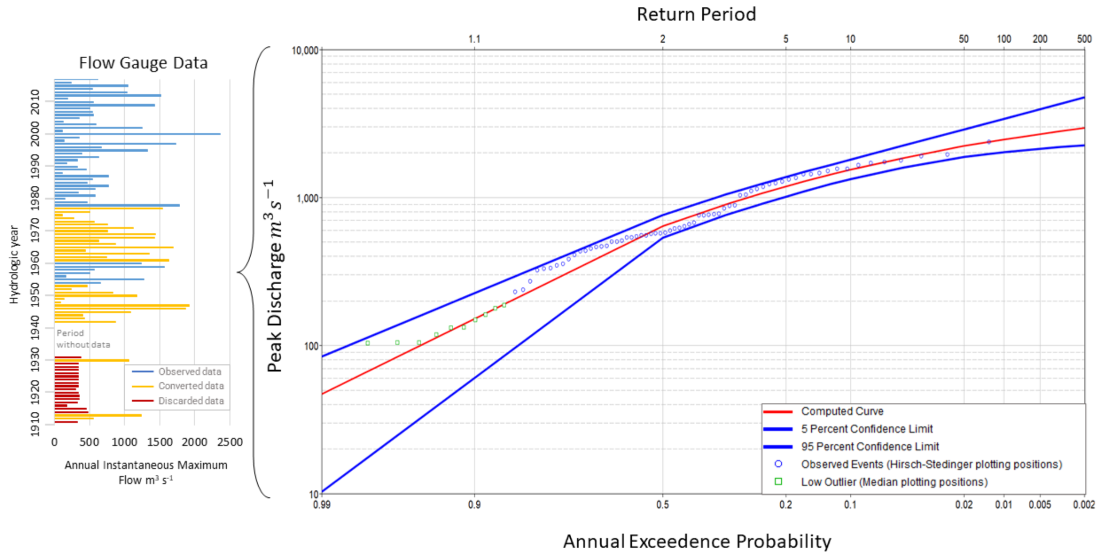

Supplementary Fig. 5. High-resolution digital model details. The geometric correction of the high-resolution digital model is illustrated via general views of the model in TIN format and an extracted hillshade from the DEM. Similarly, two cross sections taken from urban streets are displayed. The orthoimage was obtained from the Spanish National Center for Geographic Information.

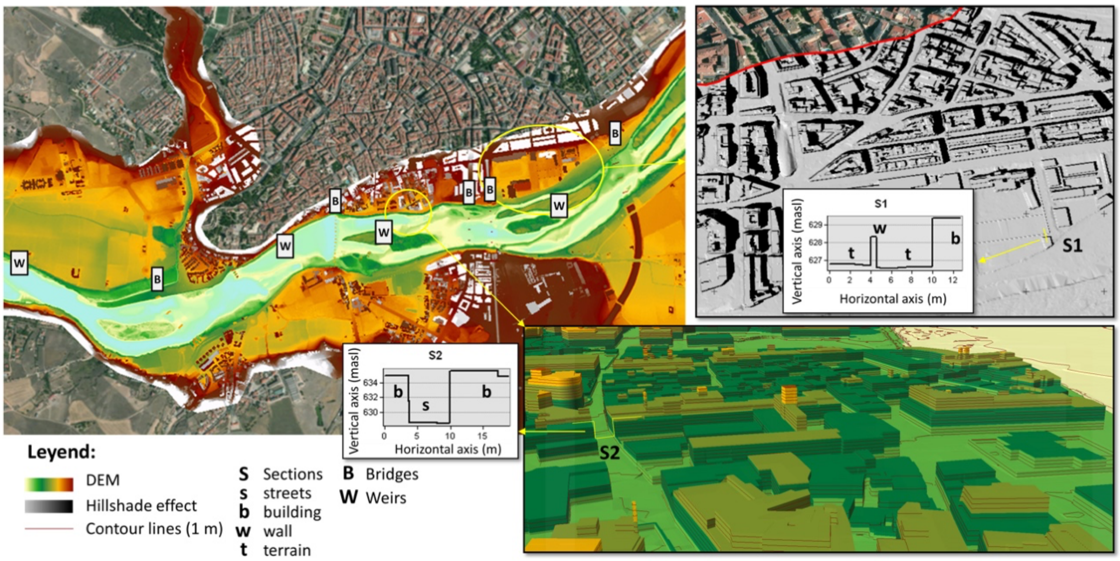

Supplementary References

[1] England, J. F. *et al*. Guidelines for Determining Flood Flow Frequency-Bulletin 17C (Ver. 1.1, May 2019): US Geological Survey Techniques and Methods, Book 4, Chap. B5. In *United States. Department of the Interior; Geological Survey (US)* (No. Techniques and Methods 4-B5). United States. Department of the Interior; Geological Survey, US, 2019).

[2] Cohn, T. A., Lane, W. L., & Stedinger, J. R. Confidence intervals for expected moments algorithm flood quantile estimates. *Water Resour. Res.* **37(6),** 1695-1706 (2001).

[3] Trancoso, A. R., Braunschweig, F., Leitão, P. C., Obermann, M., & Neves, R. An advanced modelling tool for simulating complex river systems. *Sci. Total Environ.* **407(8),** 3004-3016 (2009)

[4] Esteban-Muñoz, A. *et al*. Modeling of the river-aquifer alluvial-floodplain interaction in the reach of the Duero River between Toro and Zamora [Data set]. (Zenodo2022) https://doi.org/10.5281/zenodo.6530210

[5] Kim, J., & Scott, C. D. Robust kernel density estimation. *J Mach Learn Res.* **13(1),** 2529-2565 (2012).

[6]Scott, D.W., Multivariate Density Estimation: Theory, Practice, and visualization (John Wiley, New York, 1992).